Journal of Materials Chemistry A

Accepted Manuscript

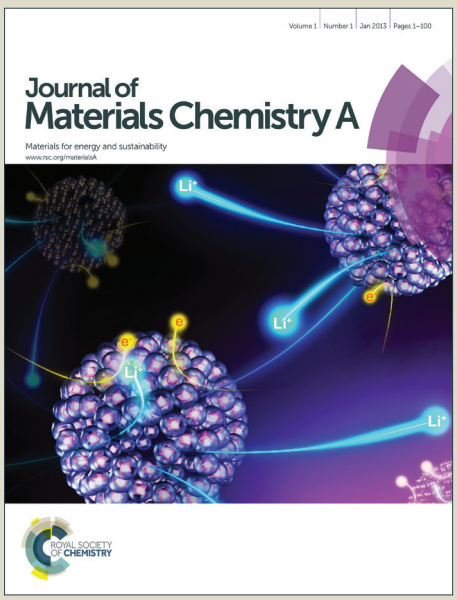

ROYAL SOCIETY OF CHEMISTRY

www.rsc.org/materialsA

Rational design of graphene/porous carbon aerogels for high-performance flexible all-solid-state supercapacitors

Hong-Fei Ju, Wei-Li Song, Li-Zhen Fan *

Institute of Advanced Materials and Technology

University of Science and Technology Beijing

Beijing, 100083, China

*Corresponding author. Tel. /fax: +86 10 62334311.

E-mail: fanlizhen@ustb.edu.cn (Li-Zhen Fan)

Abstract

Lightweight flexible energy storage devices have aroused great attention due to the remarkably increasing demand in the ultrathin and portable electronic devices. As typical new two-dimensional carbon materials, graphene-based porous structures with ultra-light weight and exclusive electrochemical properties have demonstrated outstanding capacitive ability in supercapacitors. Up to date, the performance of the all-solid-state supercapacitors achieved from graphene-based materials is still unsatisfied. In this work, we have rationally designed graphene/porous carbon (GN/PC) aerogels via a simple green strategy to achieve flexible porous electrode materials. The ordered porous carbon (PC) with high specific surface area and good capacitance was introduced as a spacer to efficiently inhibit the restacking of graphene (GN) sheets, which has significantly enhanced the specific surface area and facilitated the transport and diffusion of ions and electrons in the as-synthesized porous hybrid structure. The all-solid-state electrodes fabricated by the as-prepared GN/PC aerogels presented excellent flexibility, high specific capacitance and good rate performance in polyvinyl alcohol/KOH gel electrolyte. Implication of the specific capacitances of ~187 F g^{-1} at 1 A g^{-1} and 140 F g^{-1} at 10 A g^{-1} suggests that the GN/PC aerogels promised great potentials in the development of lightweight high-performance flexible energy storage devices.

Keywords: supercapacitor; graphene aerogel; all solid state

1. Introduction

Portable electronic devices and flexible sensor systems are highly desired in modern society, which has propelled the research on the exploration of advanced energy storage and management devices. Supercapacitor, also called electrochemical capacitors or ultracapacitors, is one of the most critical electrochemical energy-storage systems capable of meeting the rapid growing demand for clean energy generation because of their ultrahigh power density, fast charging and exceptionally long cycling life [1]. In the past decades, carbon-based materials, such as activated carbons, exfoliated carbon fibers, carbon nanotubes (CNTs) and template porous carbons, have been widely used as supercapacitor electrode materials due to their unique physical and chemical properties (high surface area , high conductivity and stability under electrochemical conditions) [2,3].

Graphene nanosheets (GN), typical two-dimensional (2D) carbon materials, have drawn great attention for their outstanding electrical and mechanical properties [4-8]. Recently, flexible graphene-based materials have become a hot topic because of their exclusive physical and chemical properties, such as large specific surface area, high conductivity and effective multidimensional pathways for electron transport [9-11]. These excellent properties have attracted increasing attention and revealed a promising path towards potential applications in supercapacitors [12-16].

Although graphene can fundamentally provide a specific capacitance up to 550 F/g [17], the specific capacitance achieved so far is still far from the theoretical value, which is largely limited by the unexpected restacking of graphene sheets. Thus, efforts have been drawn to prevent GN restacking during the formation of porous structure in order to retain the available surface and improve the electrolyte diffusion, which in turn gives rise in capacitance [18]. Various spacers, such as carbonaceous materials [19] and transition metal oxides [20], have been employed into GN to

inhibit the restacking and improve capacitive performance. For example, Chen and coworkers have utilized Co_3O_4 nanowires as the spacer to synthesize a three-dimensional (3D) graphene/Co_3O_4 nanowire hybrid structure, showing a specific capacitance of ~768 F g^{-1} at the current density of 10 A g^{-1} [21]. In spite of the greatly enhanced specific capacitance achieved by the introduction of transition metal oxides for raising pseudocapacitance, graphene/transition metal oxide composites usually suffer from low rate performance and poor stability. Therefore, carbonaceous materials in comparison could act as more promising spacers due to their relatively higher electrical conductivity and more stable structures. In the work by Chen and coworkers, CNTs were introduced as the spacer to fabricate a 3D GN/CNT aerogel [22], suggesting a high specific capacitance for the graphene component in the as-achieved supercapacitor. However, the integrated specific capacitance for GN/CNT aerogels only showed a low specific capacitance of 112 F g^{-1} mainly due to the poor specific capacitance of CNTs [23]. Recently, Lian and coworkers have developed a flexible graphene paper by introducing carbon black nanoparticles, which exhibited the maximum specific capacitance of ~136 F g^{-1} at a scan rate of 10 mV s^{-1} [24]. Although greater progresses have been made, the performance of flexible graphene materials was still unsatisfied due to the low specific capacitances of spacers. On the other hand, ordered porous carbon (PC) with high specific surface area (~710.5 m^2 g^{-1}) has presented a capacitance larger than 110 F g^{-1} (in 6 mol L^{-1} KOH) [25], which demonstrates potentials as a promising spacer for fabricating GN-based hybrid electrodes.

In addition, flexible all-solid-state supercapacitors have been widely fabricated based on their exclusive advantages in flexibility, safety and light weight to meet the requirement of rapid development in smart, ultrathin and portable electronic devices [26, 27]. Currently, polymeric gels have been largely utilized as the low-cost electrolytes in most all-solid-state supercapacitors [28-30].

For instance, Ajayan's group has fabricated all-solid-state 2D in-plane supercapacitors by using a polyvinyl alcohol (PVA)/H_3PO_4 electrolyte over the graphene electrodes, obtaining a capacitance of 247.3 F g^{-1} at 176 mA g^{-1} [31]. Shen and workers have synthesized ordered WO_3 nanowire arrays on conductive carbon cloth to fabricate high-performance flexible all-solid-state supercapacitors in PVA/H_2SO_4 electrolyte, and the as-prepared supercapacitor exhibited a high gravimetric specific capacitance of 521 F g^{-1} at 10 A cm^{-2} [32]. Although all-solid-state supercapacitors with KOH-based electrolytes have rarely been reported so far, the excellent electrochemical performance and moderate mechanical properties obtained in the PVA/KOH have demonstrated potentials in the achievement of high-performance all-solid-state electrolytes for supercapacitors [33].

In this work, we have introduced ordered porous carbon (PC) as an effective spacer to rationally design a GN/PC aerogel to take the advantages from both graphene and PC. As expected, the as-prepared GN/PC aerogels have exhibited higher capacitance than either of the individual components (GN and PC). Compared to the neat GN aerogels, the introduction of PC offers a higher specific capacitance and much enhanced rate performance (~190 F g^{-1} at a current density of 10 A g^{-1}) for the GN/PC aerogels. Furthermore, PVA/KOH gel electrolyte has been developed to fabricate flexible all-solid-state supercapacitors based on the GN/PC aerogels. A high specific capacitance of ~150 F g^{-1} at a current density of 10 A g^{-1} with excellent cycle stability was achieved. The superior performance of the GN/PC aerogels demonstrated promising applications in energy storage.

2. Experimental

Chemicals

Graphite powder was supplied by Sigma-Aldrich. Mono-dispersed SiO_2 colloidal solutions

Cataloid SI-80 (80 nm) were supplied by Catalysts & Chemicals Ind. Co. Ltd. Concentrated sulfuric acid (H_2SO_4, 98%), phenol (C_6H_6O, AR), ormaldehyde (CH_3O, AR), hydrofluoric acid (HF, 46%), sodium nitrate ($NaNO_3$, AR), potassium permanganate ($KMnO_4$, AR), hydrogen peroxide (H_2O_2, 38%), hydrochloric acid (HCl, 38%), ethanol (CH_3CHOH, AR) and ethylene glycol ($(HOCH_2)_2$, AR) were purchased from Beijing Chemicals Co. Ltd.

Synthesis of GO

Graphite oxide (GO) was synthesized according to the modified Hummers method [34]. Briefly, 2 g graphite and 1 g $NaNO_3$ were added into 120 mL of 98% H_2SO_4 in the ice bath. The solution was kept at 0 ^oC for 1 h, and then 6 g $KMnO_4$ was added gradually. After 2 h stirring, the solution was heated up to and kept at 30 ^oC for 30 min. Then, 150 mL of water was dropped slowly and 50 mL H_2O_2 (5%) was added. Finally, the solution was washed with water and HCl (5%) to obtain GO aqueous solution.

Synthesis of PC

Ordered porous carbon (PC) was prepared according to the method reported in elsewhere [35]. First, SiO_2 colloidal crystals were prepared by centrifugation of the colloidal solutions and subsequent drying. Then, the colloidal crystals were immersed in a mixed solution of phenol, aqueous ormaldehyde and a small amount of concentrated hydrochloric acid, and the mass ratio of SiO_2, PhOH and HCHO was 1.0:0.8125:0.222. After thermal treatment at 127 ^oC for 12 h in air, phenol was polymerized together with formaldehyde in the interstitial space among SiO_2 particles. Next, the interconnected phenolic resin was carbonized at 800 ^oC for 5 h in Ar atmosphere. Finally, SiO_2 templates were removed by an aqueous HF solution (46%), and the resultant porous carbons were dried under vacuum for 1 day to obtain ordered porous carbon.

Synthesis of GN/PC aerogels

Firstly, PC was dispersed in 8 mL alcohol by ultrasonication for 30 min. Then, 8 mL GO aqueous solution (2 mg/mL) was added into the PC suspension. After treated by ultrasonication for 1 h, the GO/PC solution was transferred into autoclave with a volume of 23 mL. A hydrothermal process was carried out at 180 ^{o}C for 18 h to obtain graphene/porous carbon (GN/PC) hydrogel. The as-prepared GN/PC hydrogels were washed with water and freeze-dried to achieve corresponding GN/PC aerogels. A series of GO/PC solutions with different weight ratios of GO to PC were made according to Table 1. The as-obtained neat GN aerogel was denoted as GN-EtOH. Accordingly, the GN/PC aerogels with mass ratios of 20, 10 and 5 were donated as GN/PC-20-EtOH, GN/PC-10-EtOH and GN/PC-5-EtOH, respectively.

Fabrication of supercapacitor in KOH solution

PC electrode was prepared by mixing active materials, acetylene black and polytetrafluoroethylene with the weight ratio of 80:15:5. The aerogel electrode was prepared by pressing GN-based aerogel (~2 mg) onto Ni foam without using any conductive agent and binder. A three-electrode configuration was fabricated in 6 M KOH. Hg/HgO electrode (with 1 M KOH) and Platinum foil electrode were used as reference electrode and counter electrode, respectively.

Fabrication of the all-solid-state supercapacitors

The as-prepared GN/PC aerogels were fabricated into a symmetrical all-solid-state supercapacitor. In a typical fabrication process, 4 g of PVA powder was added in 60 mL water, and the mixture was heated to 85 ^{o}C under stirring until the solution became clear. Two GN/PC electrodes were immersed in a PVA aqueous solution (10 mL), and excessive 6 M KOH solution (1000 mL) was added to soak electrodes and PVA for 24 h to obtain all-solid-state GN/PC

supercapacitors.

Material and electrochemical characterizations

The structures of the as-prepared samples were investigated by field-emission scanning electron microscopy (FESEM, ZEISS supra 55) and transmission electron microscope (TEM, FEI Tecnai G2 F30 S-TWIN). Nitrogen sorption isotherms were tested with Autosorb-iQ2-MP (Quantachrome) analyzer at 77 K. The samples were degassed at 200 ^{o}C under vacuum for more than 10 h before test. The specific surface area (S_{BET}) was calculated using the Brumauer–Emmett–Teller (BET) method. X-ray Photoelectron Spectroscopy (XPS, PHI-5300) was applied to characterize the sample surface.

The potential window was set -1–0 V (vs. Hg/HgO) in three-electrode configuration and 0–1 V in two-electrode configuration, respectively. Galvanostatic charge-discharge tests were carried out at various current densities using a LAND-CT2001A cell test instrument (Wuhan Jinnuo Electronics. Ltd.). Cyclic voltammograms (CV) and electrochemical impedance spectroscopy (EIS) data were recorded using a CHI660C electrochemical workstation (CH Instruments, Inc.). The specific capacitances of the electrodes were calculated according to the following equation:

$C = I \times t/V/m$ (in 6 M KOH electrolyte),

$C = 2 I \times t/V/m$ (in PVA/KOH gel electrolyte),

where I is the response current density (A g^{-1}), V the potential (V), m the mass of active material and t the discharge time (s).

3. Results and discussion

Upon the demonstration of graphene-CNT aerogels by Chen and co-workers [22], graphene-based aerogels can be easily prepared via the hydrothermal process. In our work, GN/PC aerogels were prepared from a stable suspension of GO and PC by a simple green approach in

alcohols. All the as-prepared GN/PC hydrogels were found to be cylindrical, and no PC particles or precipitations were observed in the residual solution when the mass ratio of PC to GN was less than 1. After freeze-drying, the shape of the GN/PC aerogels has been well retained compared to the corresponding GN/PC hydrogels. The as-obtained GN/PC aerogels also show continuous surface with high flexibility (Figure 1a). After compression, the shape and flexibility have almost been retained. Figure 1b briefly illustrates the formation of flexible GN/PC aerogels from GO aqueous solution and PC particles. The homogeneous precursor suspension was obtained by dispersing PC particles into the GO aqueous solution. Subsequently, a graphene frame with layered structures was established via self-assembly during the hydrothermal process, in which GO sheets were converted into reduced graphene oxide and PC particles were simultaneously entrapped in the graphene frame.

The as-prepared samples were characterized with different techniques and instruments. Figure 2a-2d demonstrates the typical FESEM images of PC, neat GN aerogel and GN/PC aerogels. In Figure 2a, the micro-sized macropores in the GN/PC aerogels were generated by the interconnections of GN frame. Moreover, PC aggregations have been rarely seen, indicating that PC particles have been well dispersed into the GO solution and as-prepared GN/PC aerogels. In Figure 2b, uniform ordered pores could be found in the PC particles, and the nano-sized pores in the neat GN aerogels were generated by the stacking of wrinkled graphene sheets (Figure 2c). However, the introduction of PC was found to effectively prevent graphene sheets from re-stacking in the hydrothermal process, and thus much looser structure was observed in the GN/PC aerogels (Figure 2d). The as-synthesized PC and GN/PC aerogels were performed on a TEM. According to the image in Figure 2e, the pore size of the PC was around 80 nm, and the large meso/macropore surface areas could mainly contribute to the high specific electrochemical capacitance [25]. In Figure 2f, small pieces of PC

(~400 nm) were observed to be adhered on the surface of graphene sheets and thus the stacking of GN sheets could be effectively inhibited, in good agreement with the results in the FESEM images. Therefore, the employment of PC particles into the GN aerogels would enlarge the specific surface area of the GN/PC aerogels, and on the other hand would significantly preserve the high specific surface area of the exfoliated GN. As a consequence, the barriers for the diffusion of electrolytes and ions could be largely reduced, which results in the great improvement of the capacitance for the graphene-based aerogels.

The specific surface area of the GN/PC aerogels was determined and the corresponding nitrogen adsorption-desorption isotherm curves of the GN-EtOH and GN/PC-10-EtOH were presented in Figure 3. Both the isotherms exhibit type IV isotherm with hysteresis loop, which suggests the presence of mesopores. The H4 type hysteresis loops indicate that the pores refer to the spacing formed by the stacked wrinkled graphene sheets, consistent with the results in the FESEM images. The strong adsorption observed below the relative pressure of P/P_0=0.1 in the GN/PC aerogels suggests the presence of micropores in the samples. The continuous rise of the isotherms in the relative pressure range indicates the increase in an amount of mesopores for GN/PC aerogels [16]. According to the pore distribution curves (Figure S1), it is obvious that the insertion of PC has effectively enhanced the pore volume of GN/PC aerogels (Table S1). Furthermore, S_{BET} was calculated to investigate the PC effect on the specific surface area of the GN/PC aerogels (Table S1). It is found that the specific surface area of GN/PC-10-EtOH (460 m^2 g^{-1}) was greater than the sum of the specific surface areas of GN-EtOH (406 m^2 g^{-1}) and PC (803 m^2 g^{-1}) (according to the weight ratio). Thus, the introduction of PC contributes to the enlargement of the specific surface area, which could be explained by the term of inhibiting the GN stacking.

X-ray photoelectron spectroscopy was carried out to analyze oxygen-containing species on the surface of PC, GO and GN/PC aerogels. Only carbon and oxygen were shown in the spectra (Figure 4a), and the atomic percentages of element O for PC, GO and GN/PC-10-EtOH were estimated to be 5.68 %, 30.74 %, and 11.82 %, respectively. In each XPS C1s spectrum (Figure 4b-4d), four peaks could be found to center at 284.8 eV, 286.1 eV, 287.8 eV and 289.0 eV, assigned to C–C, C–O, C=O and O–C=O species, respectively [36, 37]. In the GO sample, element O was mainly found in the form of C=O. After hydrothermal process, element O was mainly observed in the form of C–O species with a small portion of O–C=O species. In addition, some O–C=O species were also found to be formed on the surface of the graphene sheets in the hydrothermal process. According to XPS results, the formation of O–C=O and C–O species suggests the partial contribution to the self-assembly of graphene sheets. The hydrogen-bonding interaction between oxygen-containing functional groups could lead to the assembly of graphene sheets [38]. Furthermore, another factor for the formation of GN/PC aerogels may be the 3D random stacking of the flexible graphene sheets, which is mainly caused by the combination of hydrophobic and π-π interactions during the chemical reduction of GO [39].

The as-prepared GN/PC aerogels were used as integrated electrodes in the three-electrode configuration with 6 M KOH aqueous solution for electrochemical measurement. Figure 5a shows the comparison of the cyclic voltammetry (CV) curves of PC, GN aerogel and GN/PC aerogel at 50 mV s^{-1}. PC presented a regular rectangle with no obvious redox peak, which indicates a typical capacitive behaviour. Also, GN-EtOH showed a sharp distortion with an obtuse redox peak, which could be ascribed to the pesudocapacitance caused by oxygen-containing functional groups on the surface of graphene sheets. For GN/PC-10-EtOH, only a slight distortion could be observed, which

indicates that the employed PC could reduce the resistance of GN/PC-10-EtOH compared to the neat GN aerogel. Besides, we have found that the GN/PC aerogel exhibited larger current density than both PC sample and neat GN aerogel, revealing that the introduction of PC offers a higher capacitance in the GN/PC aerogel.

Electrochemical impedance spectroscopy was applied to investigate the electrical conductivity and ion transfer of the supercapacitor (Figure 5b). According to the diameter of the semicircle on the real axis in the high frequency range, the resistance of GN/PC aerogels decreased gradually with the increase of PC amount, mainly due to the smaller resistance in the PC. Moreover, all the curves at the lower region presented vertical lines paralleling to the imaginary axis, which suggests that the macro- and mesospores formed by the wrinkled graphene sheets would facilitate the electrolyte transport in the GN/PC aerogels.

In the galvanostatic charge-discharge curve (Figure 5c), the approximate isosceles triangles indicate the double layer capacitance, and the slight distortion can be ascribed to the pesudocapacitance from oxygen-containing functional groups. The specific capacitances were calculated from galvanostatic discharge curves. All the as-prepared GN/PC aerogels showed higher capacitance and better rate performance than the neat GN aerogels, suggesting the positive synergetic effect of the GN/PC hybrid.

In recent work, the spacers used for inhibiting GN stacking usually suffer from their low capacitances [22, 24]. In this work, PC with higher specific capacitance has improved the electrochemical performance as expected. Although the stacking of GN sheets has been effectively inhibited in the GN/PC aerogels, the decrease in the specific capacitance could occur when the addition amount of PC was excessive, which is mainly owing to its intrinsic lower capacitance

compared to GN. The optimal ratio of GN/PC amount for achieving the highest specific capacitance in the GN/PC aerogels was found to 10 (Figure 5d). However, further addition of PC (ratio of GN/PC>10) would result in the diminishment of specific capacitance. In all the as-prepared GN/PC aerogels, GN/PC-10-EtOH has exhibited the highest specific capacitance of 324 F g^{-1} at a current density of 0.1 A g^{-1} and ~190 F g^{-1} at 10 A g^{-1} (Figure 6a). The results are competitive to the performance of the other graphene-based supercapacitors in the recent reports [24, 40-43]. Figure 6b demonstrates the cycling performance of the device for up to 10000 cycles at a current density of 2 A g^{-1}. A small specific capacitance loss (less than 10%) was observed in the supercapacitor with GN/PC-10-EtOH electrode, indicating an excellent long-term cycling stability.

Additionally, the as-prepared GN/PC aerogels were fabricated into symmetrical all-solid-state supercapacitors (Figure 7). Typically, the GN/PC-10-EtOH was used as the electrode and the polymeric gel (PVA/KOH) electrolyte was used as both the ionic electrolyte and separator. The as-fabricated all-solid-state supercapacitor exhibited excellent mechanical flexibility and can be bent and twisted (Figure 7c).

Various characterizations were carried out to investigate the electrochemical performance of the as-fabricated all-solid-state supercapacitors. At a high scan rate of 50 mV s^{-1}, the CV curves of the flexible all-solid-state supercapacitor with GN/PC-10-EtOH electrode exhibited a nearly rectangular shape, which indicates ideal capacitive and fast charge-discharge behavior (Figure 8a). Furthermore, the EIS suggests a slight increase in the resistance, and straight lines paralleling to the imaginary axis could be still observed at the lower region of the curves, exhibiting a low ionic resistance in the PVA/KOH gel electrolyte (Figure 8b). Such low resistance in PVA/KOH is very close to the result of other PVA-based electrolytes in the recent report [29]. The specific capacitances were calculated

from the galvanostatic discharge curves. Figure 8c suggests that nearly 80 % specific capacitance was retained when GN/PC-10-EtOH was applied in the PVA/KOH electrolyte. The high specific capacitances of 272, 187, 165 and 140 F g^{-1} were obtained at a current density of 0.1, 1, 5 and 10 A g^{-1}, respectively (Figure 8c), which is highly competitive to the values found in the carbon-based all-solid-state supercapacitors (Table 2). Apparently, there is still much more room for improving the graphene-based electrodes to achieve the theoretical performance (550 F g^{-1}). More importantly, the GN/PC-10-EtOH in PVA/KOH electrolyte also exhibited excellent cycling stability (less than 10% loss after 10000 times) (Figure 8d). Compared to the performance in the transition metal oxide-based and conducting polymer-based electrodes (Table 2), such cycling stability in the GN/PC system promises more opportunities to allow them to sever in the long-term energy storage devices. The effect of mechanical bending on the electrochemical performance of GN/PC-10-EtOH in PVA/KOH electrolyte was examined based on CV test. The CV curves of the flexible supercapacitor were achieved when the supercapacitor was applied to be bent with three different bending angles (0^o, 90^o, 180^o) (Figure 9). The result suggests no meaningful change in the CV curves, revealing that the flexible GN/PC supercapacitor also presents excellent electrochemical performance even under mechanical bending. It is obvious that the as-prepared GN/PC aerogel exhibits a high level electrochemical property with a simple approach and provides huge potential as a promising electrode material for flexible all-solid-state supercapacitors.

We suggest that the excellent performance of the as-fabricated flexible all-solid-state supercapacitors could be mainly attributed to following factors. (1) Porous layered structures in the GN/PC aerogels provide large accessible surface area for charge storage. (2) Multiple channels formed by the combination of the layered GN sheets and nano-scale PC offer more electronic and

ionic diffusive paths. (3) The binder-free electrodes reduce the internal resistance to ensure fast electrode-electrolyte charge transfer. Therefore, the simple green technique coupled with the conception for enhancing electrochemical performance has demonstrated a rational design for achieving advanced flexible energy storage materials, which could be considered as a new arena in the development of ultrathin and portable electronic devices.

Conclusions

In conclusion, we have demonstrated a simple strategy to prepare mechanically robust and flexible GN/PC aerogels via the hydrothermal process. The porous layered structure in the as-prepared GN/PC aerogels provides large accessible area and effective diffusive paths to facilitate the transport and diffusion for electrolytes. The supercapacitors fabricated by GN/PC aerogels exhibited excellent electrochemical performance in the both KOH aqueous solution and PVA/KOH gel electrolyte. It is demonstrated that the as-synthesized GN/PC aerogels could be used as promising electrode materials for energy storage system.

Acknowledgements

This work was supported by the 973 project (2013CB934001), NSF of China (51172024, 51372022 and 51302011), Fundamental Research Funds for the Central Universities of China (FRF-TP-09-007A, FRF-TP-13-036A) and China PSF (2012M520165).

References

[1] P. Simon and Y. Gogotsi, Nat. Mater., 2008, 7, 845–54.

[2] L. L. Zhang and X. S. Zhao, Chem. Soc. Rev., 2009, 38, 2520–2531.

[3] M. Inagaki, H. Konno and O. Tanaike, J. Power Sources, 2010, 195, 7880–7903.

[4] K. S. Novoselov, A. K. Geim, S. V. Morozov, D. Jiang, Y. Zhang, S. V. Dubonos, I. V. Grigorieva and A. A. Filrsov, Science, 2004, 306, 666 –669.

[5] A. K. Geim, Science, 2009, 324, 1530–1534.

[6] Y. W. Zhu, S. Murali, M. D. Stoller, K. Ganesh, W. W. Cai, P. J. Ferreira, A. Pirkle, R. M. Wallace, K. A. Cychosz, M. Thommes, D. Su, E. A. Stach and R. S. Ruoff, Science, 2011, 332, 1537–1541.

[7] X. Huang, X. Y. Qi, F. Boey and H. Zhang, Chem. Soc. Rev., 2012, 41, 666 – 686.

[8] L. Z. Fan, J. L. Liu, R. Ud-Din, X. Q. Yan and X. H. Qu, Carbon, 2012, 50, 3724–3730.

[9] M. A. Worsley, P. J. Pauzauskie, T. Y. Olson, J. Biener, J. H. Satcher and T. F. Baumann, J. Am. Chem. Soc., 2010, 132, 14067–14069.

[10] Z. S. Wu, S. Yang, Y. Sun, K. Parvez, X. L. Feng and K. Müllen, J. Am. Chem. Soc., 2012, 134, 9082–9085.

[11] Z. Xu, Y. Zhang, P. Li and C. Gao, ASC Nano, 2012, 6, 7103–7113.

[12] T. Y. Kim, H. Kim, S. W. Kwon, Y. Kim, W. K. Park, D. H. Yoon, A. R. Jang, H. S. Shin, K. S. Suh and W. S. Yang, Nano Lett., 2012, 12, 743–748.

[13] D. Q. Wu, F. Zhang, H. W. Liang and X. L. Feng, Chem. Soc. Rev., 2012, 41, 6160–6177.

[14] X. W. Yang, L. Qiu, C. Cheng, Y. Z. Wu, Z. F. Ma and D. Li, Angew. Chem., Int. Ed., 2011, 50, 7325–7328.

[15] Z. S. Wu, A. Winter, L. Chen, Y. Sun, A. Turchanin, X. L. Feng and K. Müllen, Adv. Mater., 2012, 24, 5130–5135.

[16] L. L. Zhang, X. Zhao, M. D. Stoller, Y. W. Zhu, H. X. Ji, S. Murali, Y. P. Wu, S. Perales, B. Clevenger and R. S. Ruoff, Nano Lett., 2012, 12, 1806–1812.

[17] M. D. Stoller, S. J. Park, Y. W. Zhu, J. H. An and R.S. Ruoff, Nano Lett., 2008, 8, 3498 –3502.

[18] C. G. Liu, Z. N. Yu, D. Neff, A. Zhamu and B. Z. G. Jang, Nano Lett., 2010, 10, 4863–4868.

[19] M. Beidaghi and C. L. Wang, Adv. Funct. Mater., 2012, 22, 4501–4510.

[20] J. J. Liang, Y. Huang, J. Y. Oh, M. Kozlov, D. Sui, S. L. Fang, R. H. Baughman, Y. F. Ma and Y. S. Chen, Adv. Funct. Mater., 2011, 21, 3778–3784.

[21] X. C. Dong, H. Xu, X. W. Wang, Y. X. Huang, M. B. Chan-Park, H. Zhang, L. H. Wang, W. Huang and P. Chen, ACS Nano, 2012, 6, 3206–3213.

[22] Y. Wang, Y. P. Wu, Y. Huang, F. Zhang, X. Yang, Y. F. Ma and Y. S. Chen, J. Phys. Chem. C, 2011, 115, 23192–23197.

[23] E. Frackowiak, K. Metenier, V. Bertagna and F. Beguin, Appl. Phys. Lett., 2000, 77, 2421–2423.

[24] G. Wang, X. Sun, F. Lu, H. Sun, M. Yu, W. Jiang, C. Liu and J. Lian, Small, 2012, 8, 452–459.

[25] L. Z. Fan, S. Y. Qiao, W. L. Song, M. Wu, X. B. He and X. H. Qu, Electrochim. Acta, 2013, 105, 299–304.

[26] K. Wang, W. J. Zou, B. G. Quan, A. F. Yu, H. P. Wu, P. Jiang and Z. X. Wei, Adv. Funct. Mater., 2011, 1, 1068–1072.

[27] M. Kaempgen, C. K. Chan, J. Ma, Y. Cui and G. Gruner, Nano Lett., 2009, 9, 1872–1876.

[28] M. F. El-Kady, V. Strong, S. Dubin and R. B. Kaner, Science, 2012, 335, 1326–1330.

[29] Y. X. Xu, Z. Y. Lin, X. Q. Huang, Y. Liu, Y. Huang and X. F. Duan, ACS Nano, 2013, 7, 4042–4049.

[30] F. H. Meng and Y. Ding, Adv. Mater., 2011, 23, 4098–4102.

[31] J. J. Yoo, K. Balakrishnan, J. S. Huang, V. Meunier, B. G. Sumpter, A. Srivastava, M. Conway, A. L. M. Reddy, J. Yu, R. Vajtai and P. M. Ajayan, Nano Lett., 2011, 11, 1423–1427.

[32] L. N. Gao, X. F. Wang, Z. Xie, W. F. Song, L. J. Wang, X. Wu, F. Y. Qu, D. Chen and G. Z. Shen, J. Mater. Chem. A, 2013, 1, 7167–7173.

[33] A. Lewandowski, K. Skorupska, J. Malinska, Solid State Ionics, 2000, 133, 265–271.

[34] W. Hummers and R. O fleman, J. Am. Chem. Soc., 1958, 80, 1339.

[35] H. Yamada, H. Nakamura, F. Nakahara, I. Moriguchi and T. Kudo, J. Phys. Chem. C, 2007, 111, 227–233.

[36] Y. Zhou, Q. Bao, L. A. L. Tang, Y. Zhong and K. P. Loh, Chem. Mater., 2009, 21, 2950–2596.

[37] S. Stankovich, D. A. Dikin, R. D. Piner, K. A. Kohlhaas, A. Kleinhammes, Y. Jia, Y. Wu, S. T. Nguyen and R. S. Ruoff, Carbon, 2007, 45, 1558–1565.

[38] Y. X. Xu, K. X. Sheng, C. Li and G. Q. Shi, ACS Nano, 2010, 4, 4324–4330.

[39] C. Huang and P. S. Grant, Sci. Rep., 2013, 3, 2393.

[40] S. Hu, R. Rajamani and X. Yu, Appl. Phys. Lett., 2012, 100, 104103.

[41] S. Wang and R. A. W. Dryfe, J. Mater. Chem. A, 2013, 1, 5279–5283.

[42] B. G. Choi, S. J. Chang, H. W. Kang, C. P. Park, H. J. Kim, W. H. Hong, S. G. Lee and Y. S. Huh, Nanoscale, 2012, 4, 4983–4988.

[43] M. F. El-Kady, V. Strong, S. Dubin and R. B. Kaner, Science, 2012, 335, 1326–1330.

[44] K. Z. Gao, Z. Q. Shao, J. Li, X. Wang, X. Q. Peng, W. J. Wang and F. J. Wang, J. Mater. Chem. A, 2013, 1, 63–67.

[45] Y. J. Kang, S. J. Chun, S. S. Lee, B. Y. Kim, J. H. Kim, H. Chung, S. Y. Lee and W. Kim, ACS Nano, 2012, 6, 6400–6406.

[46] X. Xiao, X. Peng, H. Y. Jin, T. Q. Li, C. C. Zhang, B. Gao, B. Hu, K. F. Huo and J. Zhou, Adv. Mater., 2013, 25, 5091–5097.

[47] L. Y. Yuan, X. H. Lu, X. Xiao, T. Zhai, J. J. Dai, F. C. Zhang, B. Hu, X. Wang, L. Gong, J. Chen, C. G. Hu, Y. X. Tong, J. Zhou and Z. L. Wang, 2012, ACS Nano, 6, 656–661.

[48] X. Xiao, T. Q. Li, P. H. Yang, Y. Gao, H. Y. Jin, W. J. Ni, W. H. Zhan, X. H. Zhang, Y. Z. Cao, J. W. Zhong, L. Gong, W. C. Yen, W. J. Mai, J. Chen, K. F. Huo, Y. L. Chueh, Z. L. Wang and J. Zhou, ACS Nano, 2012, 6, 9200–9206.

[49] J. Y. Tao, N. S. Liu, W. Z. Ma, L. W. Ding, L. Y. Li, J. Su and Y. H. Gao, Sci. Rep., 2013, 3, 2286.

[50] C. Z. Meng, C. H. Liu, L. Z. Chen, C. H. Hu and S. S. Fan, Nano Lett., 2010, 10, 4025–4031.

1 **Table caption**

2 Table 1 Composition of GO/PC solutions for preparing GN/PC aerogels.

3 Table 2 Electrochemical performance of the all-solid-state supercapacitors in recent literatures.

4

1 Table 1

Sample	Mass of GO (mg)	Mass of PC (mg)	alcohol	Ratio of GN to PC
GN-EtOH	16	0	EtOH	-
GN/PC-20-EtOH	16	0.5	EtOH	20
GN/PC-10-EtOH	16	1	EtOH	10
GN/PC- 5 -EtOH	16	2	EtOH	5

2

3

1 Table 2

Electrode materials for all-solid-state supercapacitors	Specific capacitance	Electrolytes	Cycling stability (cycling number, cycling current density)	Refs.
GN/PC aerogels	272 F g^{-1} (at 0.1 A g^{-1}) 187 F g^{-1} (at 1 A g^{-1}) 165 F g^{-1} (at 5 A g^{-1}) 140 F g^{-1} (at 10 A g^{-1})	PVA/KOH	>90% (10000, 2 A/g)	this work
Graphene hydrogel	186 F g^{-1} (at 1 A g^{-1})	PVA/H_2SO_4	92% (10000, 10 A/g)	[29]
Laser scribed graphene	204 F g^{-1} (at 1 A g^{-1})	PVA/H_3PO_4	~97% (10000)	[44]
Graphene films	247 F g^{-1} (at 176 mA g^{-1})	PVA/H_3PO_4	~95% (1500, 176 mA g^{-1})	[31]
Cellulose nanofiber–graphene	207 F g^{-1} (at 5 mV s^{-1})	PVA/H_2SO_4	99% (5000, 3.4 mA cm^{-2})	[45]
Nanotube/bacterial nanocellulose papers	47 F g^{-1} (at 100 mV s^{-1})	Ionic liquid polymer gel	>99.5% (10000, 10 A g^{-1})	[46]
MWNT-ionomer	91 F g^{-1} (at 150 mV s^{-1})	Nafion Membranes	88% (2000, 2 A g^{-1})	[40]

Polypyrrole/decorated nanoporous gold	270 F g^{-1} (at 0.6 A g^{-1})	PVA/$HClO_4$	-	[30]
Vanadium nitride/CNT	7.9 F cm^{-3} (at 25 mA cm^{-3})	PVA/H_3PO_4	82% (10000, 0.2 A cm^{-3})	[47]
Carbon nanoparticles /MnO_2 nanorods	4.8 Wh kg^{-1} (at 14 kW kg^{-1})	PVA/H_3PO_4	97.3% (10000, 1 mA cm^{-2})	[48]
Carbon/MnO_2 coreshell fiber	2.5 F cm^{-3} (at 0.02 A cm^{-3})	PVA/H_3PO_4	84% (10000, 0.1 Acm^{-3})	[49]
WO_3 nanowire arrays/carbon cloth	521 F g^{-1} (at 1 A g^{-1})	PVA/H_2SO_4	-	[32]
PPy-MnO_2-carbon composites	69.3 F cm^{-3} (at 0.1 A cm^{-3})	PVA/H_3PO_4	86.7% (1000, 1 A cm^{-3})	[50]
Polyaniline/CNT	332 F g^{-1} (at 1 A g^{-1})	PVA/H_2SO_4	91.9% (1000, 1 A g^{-1})	[51]

Figure captions:

Figure 1 (a) Recovery of GN/PC-10-EtOH after compression; (b) Illustration of the formation of GN/PC aerogel.

Figure 2 Typical FESEM images of (a) the graphene frame in GN/PC-10-EtOH, (b) PC and the magnified images of graphene frame in (c) GN-EtOH and (d) GN/PC-10-EtOH; Typical TEM images of (e) PC and (f) GN/PC-10-EtOH.

Figure 3 N_2 adsorption−desorption isotherms of GN-EtOH and GN/PC-10-EtOH.

Figure 4 (a) XPS survey plots of PC, GO and GN/PC-10-EtOH; C1s spectra for (b) PC, (c) GO and (d) GN-PC-10-EtOH.

Figure 5 (a) CV curves of PC, GN-EtOH and GN/PC-10-EtOH at 50 mV s^{-1} scan rate; (b) Nyquist plots for different samples based supercapacitors at a DC bias of 0 V with a sinusoidal signal of 10 mV over the frequency range 100 kHz to 0.01Hz; (c) Typical galvanostatic charge/discharge curves of GN/PC-10-EtOH electrode at different current densities in KOH; (d) Specific capacitances of GN/PC aerogels with different ratios.

Figure 6 (a) Specific capacitances of PC, GN-EtOH and GN/PC-10-EtOH in KOH. (b) The cycling stability of GN/PC-10-EtOH in KOH.

Figure 7 (a) Illustration of the fabrication of all-solid-state supercapacitors; (b) All solid-state GN/PC-10-EtOH supercapacitor; (c) The flexibility of the all-solid-state supercapacitor.

Figure 8 (a) CV curves of GN/PC-10-EtOH in PVA/KOH gel electrolyte; (b) Nyquist plots for GN/PC-10-EtOH in PVA/KOH gel electrolyte at a DC bias of 0 V with a sinusoidal signal of 10 mV over the frequency range 100 kHz to 0.01Hz; (c) Specific capacitance of GN/PC-10-EtOH in PVA/KOH gel electrolyte; (d) The cycling stability of GN/PC-10-EtOH in PVA/KOH gel electrolyte.

Figure 9 CV curves for all-solid-state supercapaciotor of GN/PC-10-EtOH bent with different angles (0^o, 90^o, 180^o).

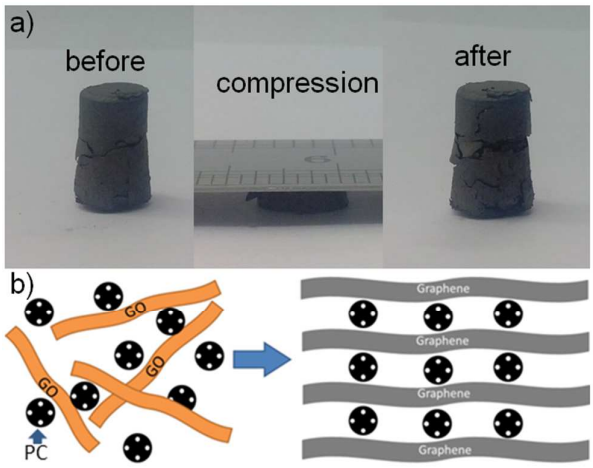

Figure 1

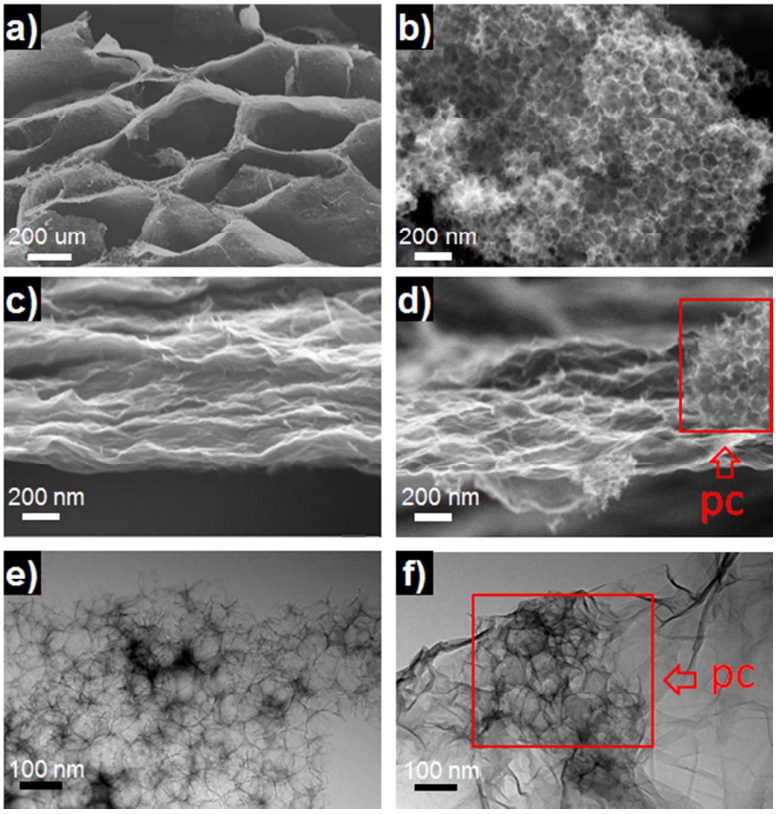

Figure 2

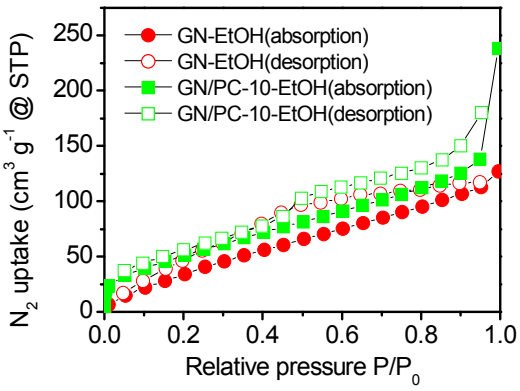

Figure 3

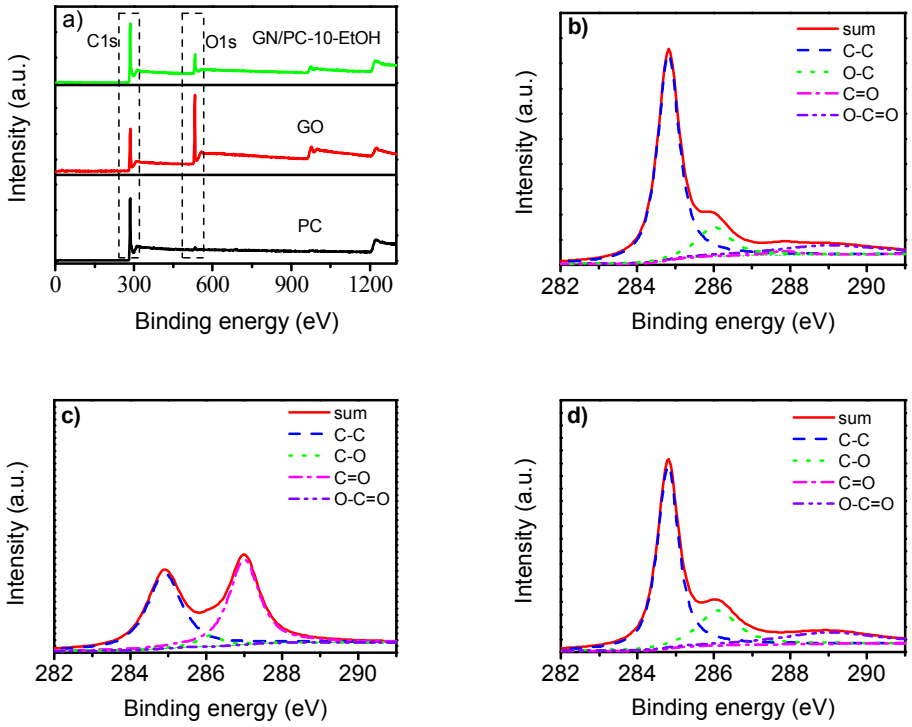

Figure 4

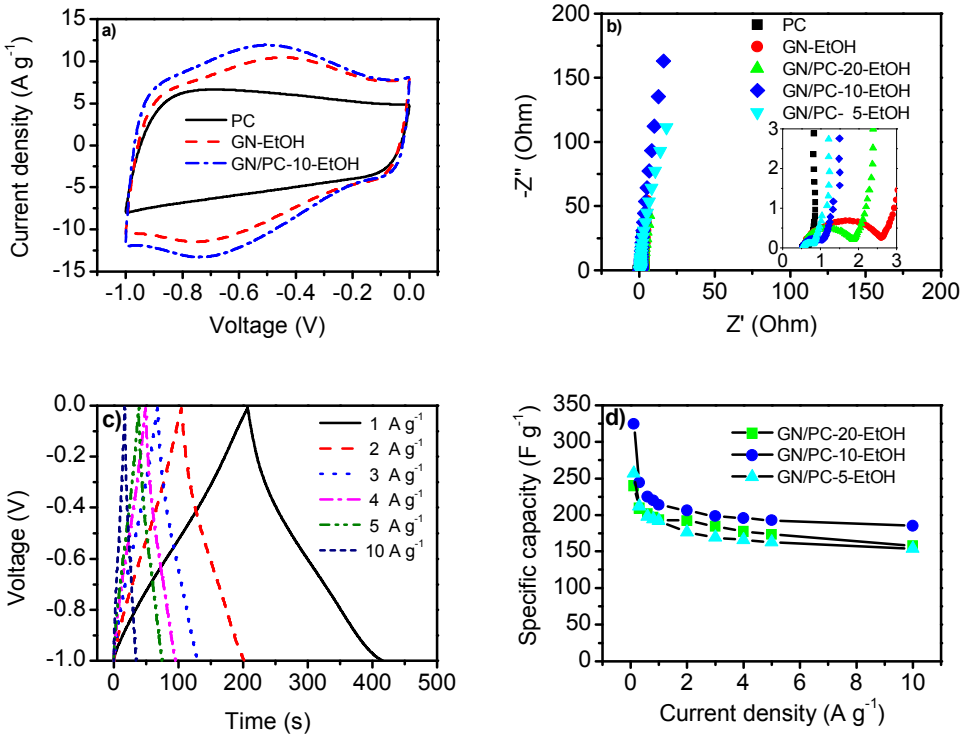

Figure 5

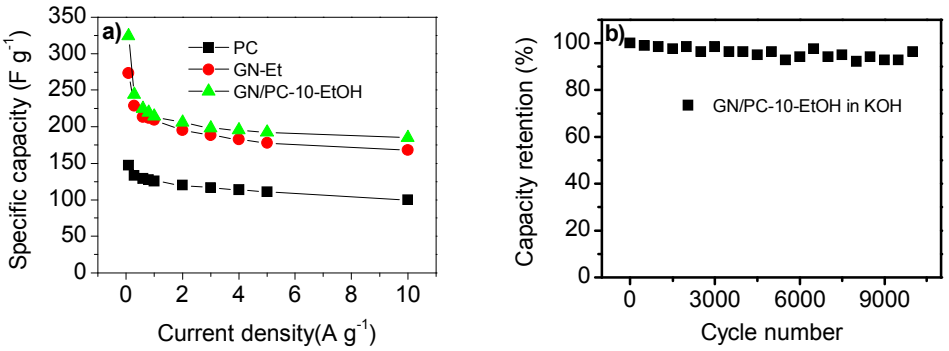

Figure 6

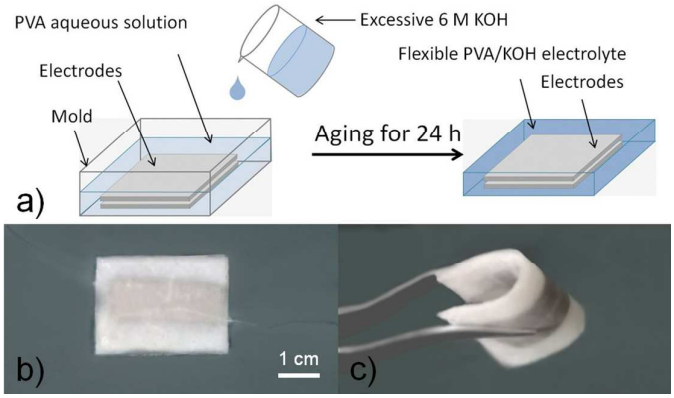

Figure 7

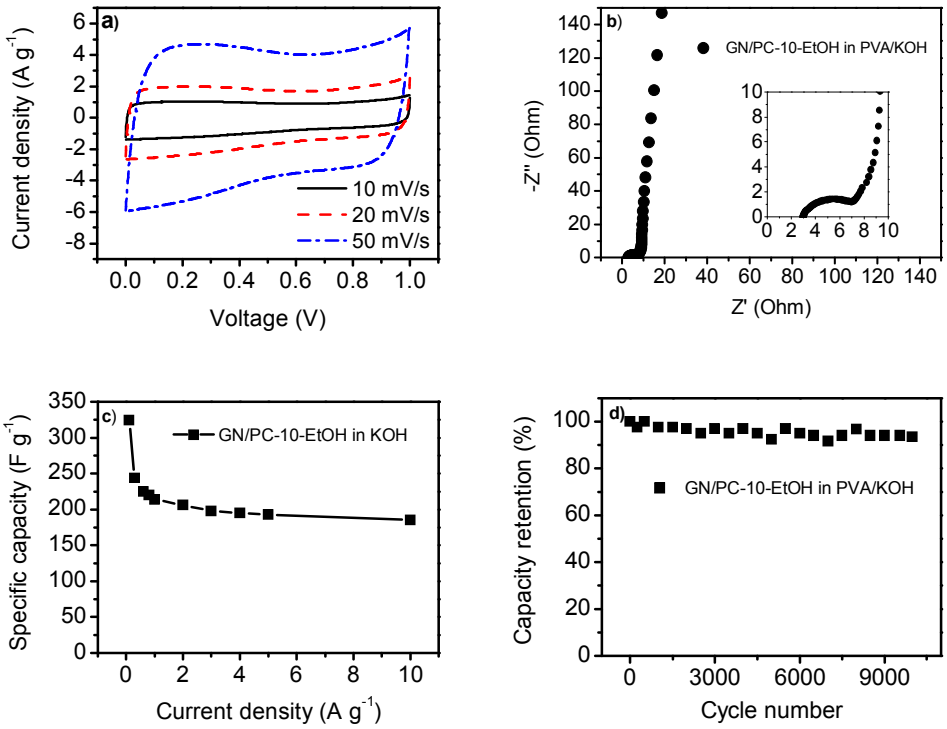

Figure 8

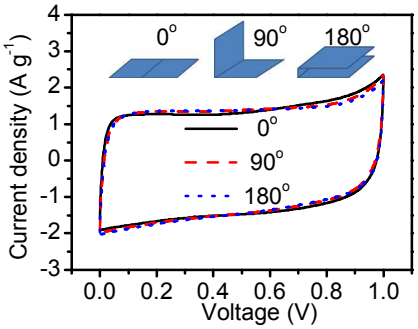

Figure 9